JOURNAL OF MATERIALS SCIENCE 17 (1982) 878–884

Slip systems in gadolinium gallium garnet single crystals

H. GAREM, J. RABIER, P. VEYSSIERE
Laboratoire de Métallurgie Physique, 40 Avenue du Recteur Pineau, 86022 Poitiers, France

$Gd_3Ga_5O_{12}$ single crystals with compression axes of different orientations have been deformed under creep conditions in air at 1450° C and 1550° C (0.86 T_M and 0.92 T_M, respectively, where T_M is the melting temperature). After a few per cent of permanent strain the deformation substructure has been studied by optical and transmission electron microscopy. Etching and bi-refringence patterns indicate that slip on {1 1 0}, {1 1 2} and {1 2 3} can be activated depending on the orientation of the compression load. Dislocations with $\frac{a}{2}$ ⟨1 1 1⟩ Burgers vectors have been observed to glide in {1 1 0} planes. They exhibit a segmented aspect suggesting their dissociation out of the glide plane.

1. Introduction

Gadolinium gallium garnet (GGG; $Gd_3Ga_5O_{12}$) is the standard substrate material required for epitaxial growth of single-crystal iron garnet films used in magnetic bubble domain technology. As a consequence, large single crystals are now available with dislocation densities less than 1 cm^{-2}. With regard to the increasing demand for materials with high melting point and good mechanical properties at high temperature for structural applications, the plastic properties of GGG have to be investigated. Indeed, this compound possesses a high melting temperature (1720° C) and the garnet structure, a complex cubic structure with no close-packed plane in the oxygen sub-lattice, and so should show good mechanical properties since the dislocations have to overcome high lattice friction stresses [1].

This paper reports a preliminary study of the high-temperature deformation of GGG single-crystals focussed on the characterization of the glide systems and of the properties of dislocations.

2. Mechanical tests

Parallelepiped samples (2 mm x 2 mm x 5 mm) with ⟨0 0 1⟩, ⟨0 1 1⟩ and ⟨1 1 1⟩ compression axes were cut from a Czochralski boule of GGG (from Union Carbide, San Diego, CA) with a dislocation density of about 1 cm^{-2}. The lateral faces were oriented and mechanically polished with diamond pastes such that the etching conditions were optimized [2] (see Section 3.2).

Samples were deformed in a creep machine working in air up to 1800° C [3]. The deformation was recorded at the specimen ends through sapphire rods used as sensors.

GGG single crystals proved to possess a particularly high mechanical strength. In order to achieve plastic deformation, creep tests have been conducted at elevated temperatures, T ($T > 1400°$ C). At these temperatures significant deformations are only obtained under rather large stress, σ, levels ($\sigma > 200$ MPa).

As opposed to the usual primary stage, generally related to a hardening process, the creep curves, $\epsilon(t)$, exhibit a shape typical of that of crystals having a low density of mobile dislocations (Fig. 1), as expected. These curves display an acceleration of the strain-rate related to dislocation multiplication. No decrease in creep-rate up to $\epsilon = 0.15$ has been detected, which would have been indicative of a hardening mechanism. Furthermore, microscopic cracks cannot be prevented from appearing in the samples at high deformations.

The creep curves are consistent with the fact that the multiplication of fresh dislocations is difficult in these crystals; this was already noticed in other samples with garnet structure as in natural

0022–2461/82/030878–07$03.34/0

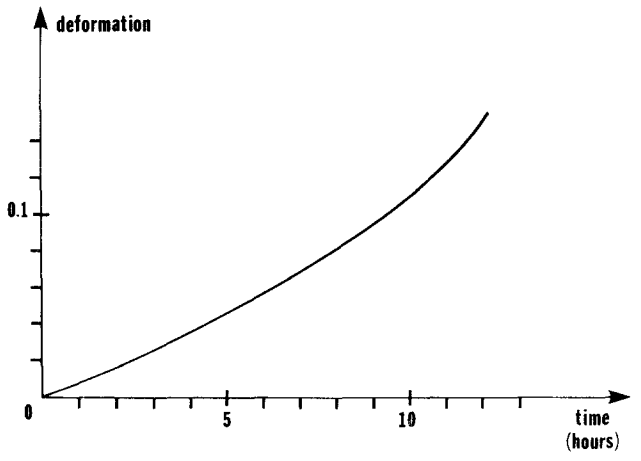

Figure 1 Example of a creep curve showing no indication of hardening up to 13% strain. ($T = 1550°$ C, $\sigma = 200$ MPa, load axis [001]).

garnet or as in $Y_3Fe_5O_{12}$ [1, 4]. This point will be illustrated by TEM observations in Section 4.

In the following, the deformation substructure of GGG single-crystals deformed at high temperature is reported. However, the present analysis will be restricted to the early stages of deformation ($\epsilon \lesssim 0.02$), a situation which is likely to provide only a moderate increase in internal stresses and, in turn, a reduced chance that the dislocation substructure has evolved through a recovery process during the cooling procedure [5]. In other words, such a procedure is anticipated to provide configurations almost free from undesirable recovery, that is featuring the state of deformation at elevated temperature with reduced ambiguity.

3. Surface analysis

Two optical techniques, the observation of surface etch pits and of stress-induced bi-refringence patterns of samples examined in transmission were employed to obtain independent determinations of the glide systems. However, after high temperature deformation in air, the observations were perturbed by the presence of changes in the surface condition of the specimens.

3.1. Superficial exsolution

Since a similar change was found on the surface of GGG samples annealed at the same temperature as that of the deformation tests ($T > 1400°$ C, see Fig. 2a), the effect is not strain-related; it is localized at the surface for it disappears after mechanical grinding. Images of these alterations with the $K\alpha_1$ peaks of Ga and Gd on a CAMECA electron microprobe reveal that the structures produced are almost free of Ga (Fig. 2b) but are probably Gd oxide precipitates (Fig. 2c). It was not possible, however, to determine their crystal structure by X-ray diffraction.

The occurence of this effect is not yet understood. Similar surface features have been found in $Y_3Fe_5O_{12}$ [1, 6]: the iron-rich second phase present on the surface after high-temperature annealing has been attributed in this case to the evaporation of flux impurities during the heat treatment [6], resulting in a local excess of iron in the garnet matrix and in its subsequent precipitation as an iron-rich phase. In GGG, however, since the single crystal was grown by the Czochralski method it is not thought to contain an impurity level comparable to that found in flux-grown crystals, the surface second-phase might be related to growth heterogeneities which are known to be responsible for the so-called growth striations perpendicular to the ⟨111⟩ growth axis. These striations are associated with departures from the molecular composition [7]. The regions of the samples enriched with gadolinium, could yield a Gd oxide by a diffusion process, since the domain of garnet solid soultion is very narrow in composition [8]. However, no unambiguous 1 : 1 relation between growth striations and the Gd-rich second phase in GGG has been observed.

3.2. Glide systems

After deformation, the surfaces of the samples were mechanically ground away to a depth of a few micrometres to remove the second phase and subsequently polished using 3 μm and 0.25 μm grade diamond pastes. The surfaces were then etched in order to reveal the points of emergence of the dislocations using a 1 : 1 mixture (by volume) of concentrated H_2SO_4 and H_3PO_4 at 165° C [2]. The slip planes were determined from the obser-

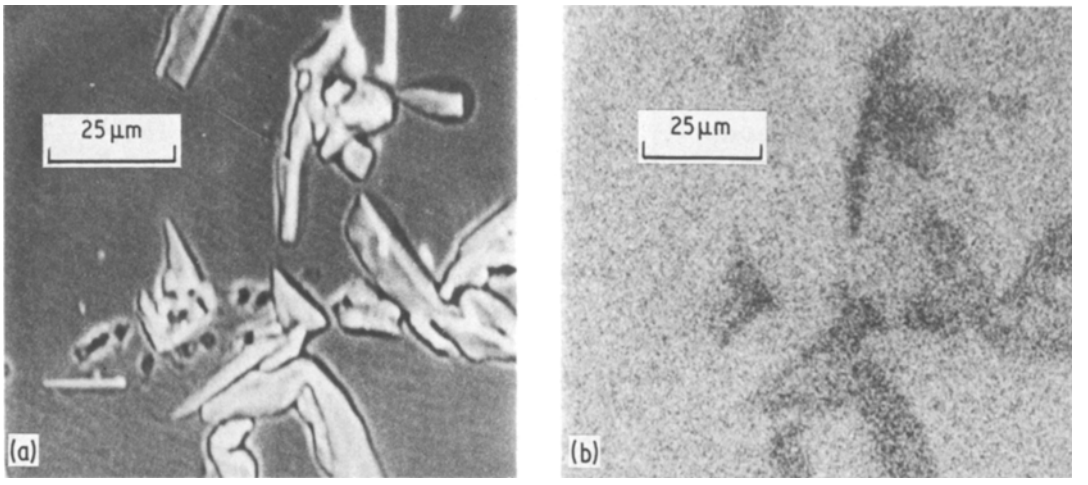

Figure 2 Electron microprobe images under different imaging conditions showing the presence of a superficial second phase on the GGG samples deformed at 1450° C: (a) absorbed electrons (b) Ga ($k\alpha_1$) peak and (c) Gd ($k\alpha_1$) peak.

vation of etch pit alignments, indicative of slip plane traces, when present in reproducible amounts (see Fig. 3a).

Stress-induced bi-refringence patterns were also used to study the stress distribution in the bulk. It was found that, before deformation, growth striations along {1 1 1} are clearly visible, whereas, after deformation growth striations tend to disappear. The directions of stress heterogeneities in the bi-refringence patterns are fully consistent with the orientation drawn from etch pitting (Fig. 3a and b).

The glide planes operating during high temperature deformation of GGG, e.g. {1 1 0}, {1 1 2} and {1 2 3}, are those usually observed in bcc metals, the activation of the different planes being related, here, to the shear stress acting on them through the orientation of the load axis (see Fig. 3 and Table I). These planes are not equivalent in so far as glide is concerned, since the glide plane with the highest Schmid factor is not systematically activated; furthermore, comparison of the data obtained for two distinct orientations of the compression axis, e.g. [0 0 1] and [$\bar{1}$ 1 0], shows that, surprisingly, the activation of a given glide plane is not controlled by the Schmid factor on this plane only. The situation is indeed a rather particular one, since the same Schmid factors on the same plane yields opposite observations. The critical resolved shear stresses, τ, on the different planes must be of the same order of magnitude, that on {1 1 0} being slightly lower than that on the other possible glide planes ($\tau_{110} \sim 0.9\,\tau_{112}$); the basic reasons for this behaviour are to be studied further on the TEM scale.

The deformation substructure revealed by the etch-pit distribution on the lateral faces shows an important density of dislocations close to the compression faces of the samples (Fig. 3) where deformation by glide is generally absent; indeed, it is generally considered that the glide planes which intersect surfaces constrained by contact with the deformation rods cannot be activated during the deformation, this defining a cone of no deformation at each end of the compressed samples (dead zones). However, as already discussed in the case of inverted barrel-like samples [1, 9], the presence of this unexpected density of etch pits might be related to the nucleation of dislocation sources

TABLE I Results of the analysis of slip traces depending upon the direction of the compressive load

Compression axis	Potential glide plane $\{h\,k\,l\}$	Schmid factor on $\langle 111\rangle\{h\,k\,l\}$	Glide planes experimentally observed
[001]	{112}	0.47	
	{123}	0.46	
	{110}	0.41	(011) (101) (01$\bar{1}$) ($\bar{1}$01)
[$\bar{1}$10]	{112}	0.47	(1$\bar{1}$2) ($\bar{1}$12)
	{123}	0.46	($\bar{1}$23) (2$\bar{1}$3)
	{110}	0.41	
[111]	{112}	0.32	(112)
	{123}	0.31	(123)
	{$\bar{1}$10}	0.27	(110)

operating by climb, even in these early stages of deformation. On the other hand, the deformation in the central part of the samples is inhomogeneous and takes place in only a few narrow glide bands which shows that climb is not important enough to promote a fully rearranged dislocation cell substructure (see Fig. 4).

4. TEM observations of deformation sub-structures

Observation only of specimens with [001] compression axis is presented in this preliminary study. Sections were cut parallel to the activated (011) glide plane, subsequently mechanically ground and eventually ion-thinned. The thin foils were mostly studied in a Philips EM 300 electron microscope operating at 100 kV.

Dislocation loops developing by glide are the typical feature of the deformation substructure in GGG at this level of strain ($\epsilon < 0.02$) and temperature ($T > 1400°$ C). Their Burgers vectors are of the type $\frac{a}{2}\langle 111\rangle$ which is the shortest unit translation in the garnet structure. Dislocation junctions with a $\langle 100\rangle$ Burgers vectors have also been observed. There is good agreement between these Burgers vectors and others determined in yttrium–iron garnet [10, 11].

Fig. 5 shows an example of the dislocation

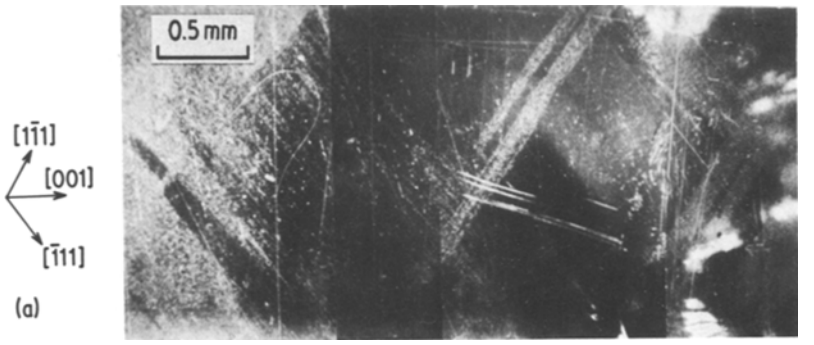

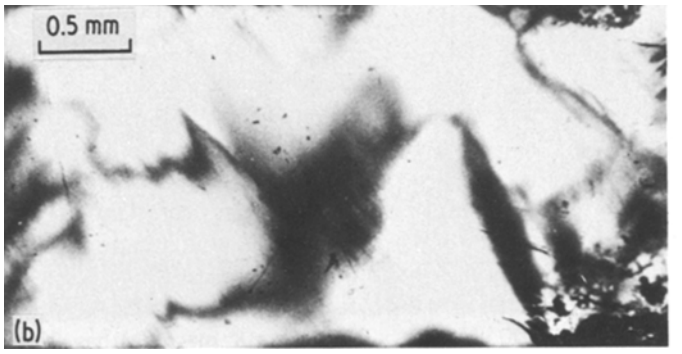

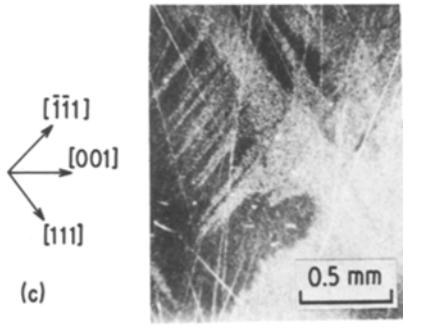

Figure 3 Optical observation of a sample deformed along [001] ($T = 1550°$ C, $\epsilon \sim 0.016$) showing a comparison between (a) chemical etch pits on (110) (b) bi-refringence pattern of the same face and (c) etch pits on ($\bar{1}$10).

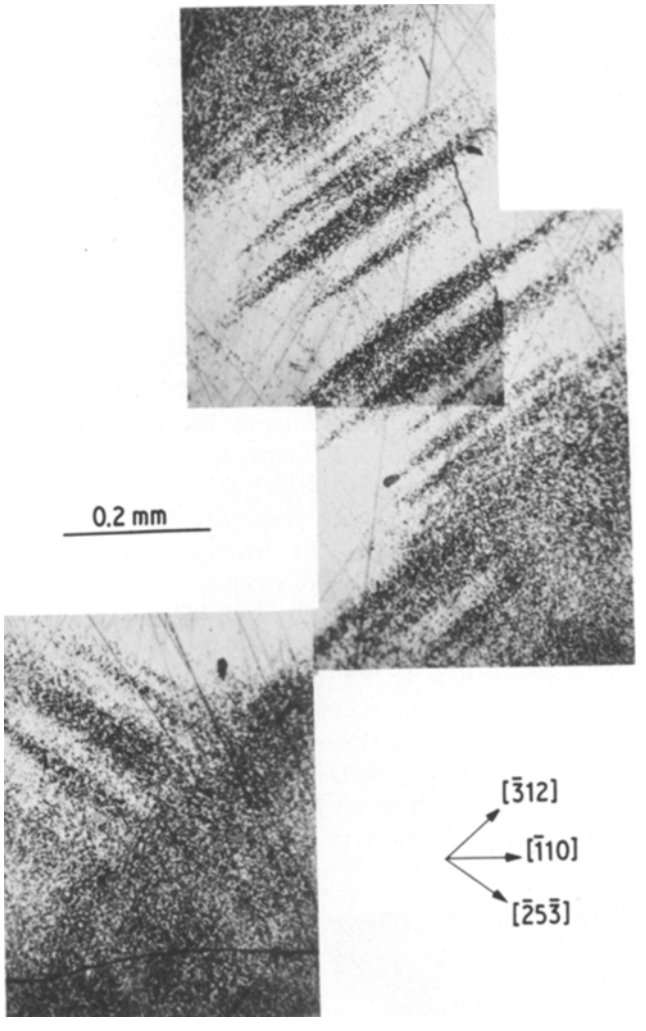

Figure 4 Etch pits on the central part of a GGG sample deformed along [1$\bar{1}$0]. (T = 1450° C, $\epsilon \sim 0.025$).

substructure. It consists of two dislocation segments with opposite Burgers vectors ($\pm \frac{a}{2}$ [11$\bar{1}$]) bowed-out in two parallel (011) planes. The expansion of these two glide loop segments has been stopped by the attractive interaction of their leading parts. Further evolution of this configuration requires either a larger applied stress in order to overcome the long-range attractive stress or the activation of cross-slip of the screw segments or climb of the others, so that the dislocations with opposite sign would annihilate. This configuration provides good evidence of the operation of the $a/2$ ⟨111⟩ {110} glide system, consistent with the macroscopic determination of slip traces (see Section 3.2.).

In addition, it is worth mentioning that these dislocation loop segments exhibit straight sections, oriented along well-defined simple crystallographic orientations ([2$\bar{1}$1], [110] and [$\bar{1}\bar{1}$1] in Fig. 5). This segmentation may be ascribed to Peierls stresses which are expected to be unusually high in such materials. Indeed, the glide planes are very rough on a hard sphere model. The fact that the dislocations might be dissociated out of their glide plane could be another explanation for this effect. The effect of anisotropy on line energy through that of the elastic constants, C_{ij}, can be ruled out since the anisotropy factor, A, is very close to unity ($A = 2C_{44}/(C_{11} - C_{12}) = 1.05$ [12]).

Images under weak-beam conditions have failed to reveal a dissociation of these dislocations except of their screw parts which seem to be dissociated into two partials (Fig. 6). A more detailed TEM study is in progress with particular attention being given to the possible climb dissociation, as in yttrium–iron garnet. Re-examination of the dislocation substructures at higher voltages (up to 200 kV with a JEOL 200 CX machine) has shown

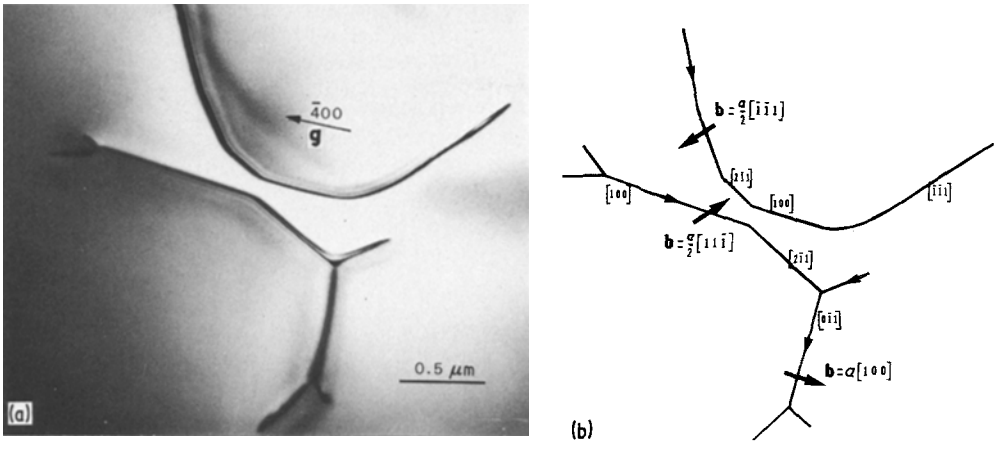

Figure 5 Dislocation segments gliding in (0 1 1) (see text) showing (a) Bright-field micrograph (the multiple images are due to the difficulty of obtaining two-beam images), and (b) Schematical representation containing the results of the analysis of contrast and orientations of the various dislocation segments.

that dislocation could be heavily affected by irradiation defects created during the observation. The major resulting features are the creation of small dislocation loops and a widening of the dissociation which can be eventually detected in the non-screw parts.

5. Conclusion

A preliminary characterization of the mechanical strength of GGG has been carried out. It is found that relatively high stresses are required to induce plastic deformation by creep even at temperatures close to the melting point (0.92 T_M). This high resistance to plastic deformation seems to be a general trend in crystals with the garnet structure.

The observed glide planes are identical to these usually found in bcc crystals, e.g. {1 1 0}, {1 1 2} and {1 2 3}; the analogy based on comparable crystals symmetries also holds for the Burgers vectors which are of the $a/2\langle 1\,1\,1\rangle$-type, at least for dislocations gliding in {1 1 0}.

Creep curves and TEM observations support the idea of fairly high lattice friction stresses which oppose to the movement of dislocations and render their multiplication difficult.

Dissociated screw segments have probably been observed; however, the occurrence of climb dissociated non-screw parts which, as in yttrium–iron garnet, would explain the segmented aspect they exhibit, is still a matter of investigation.

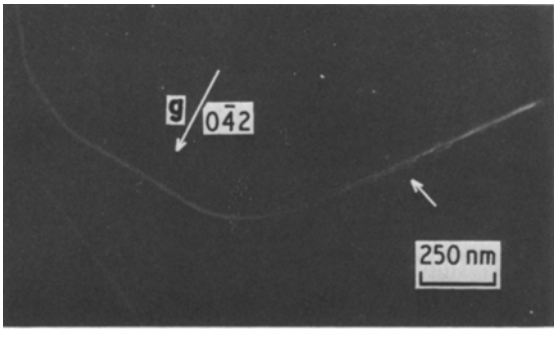

Figure 6 Dark-field image of a detail of the configuration in Fig. 5 ($\mathbf{g} = 0\bar{4}2$, $S_g = 4.10^{-2}\,nm^{-1}$). The contrast suggests that the screw part of the dislocation exhibits segments alternatively dissociated and constricted.

Acknowledgements

The authors gratefully acknowledge the assistance of R. J. Gaboriaud, J. P. Guillot and E. L. Mathe, during the creep tests, X-ray diffraction and electron microprobe analysis, respectively.

References

1. J. RABIER, Thèse de Doctorat, Poitiers (1979).
2. J. W. MATTHEWS, E. KLOKHOLM, V. SADAGOPAN, T. S. PLASKETT and E. MENDEL, *Acta Metall.* **21** (1973) 203.
3. R. J. GABORIAUD, Thèse de Doctorat, Poitiers (1978).
4. J. RABIER, P. VEYSSIÈRE and H. GAREM, *Phil. Mag.* to be published.
5. T. BRETHEAU, J. CASTAING, J. RABIER and P. VEYSSIÈRE, *Adv. Phys.* **28** (1979) 829.
6. W. T. STACY, M. A. H. HUYBERTS, R. METSELAAR and A. B. VOERMANS, *J. Appl. Phys.* **48** (1977) 4766.
7. R. HERGT, M. WENDT, P. GÖRNERT and S. BORNMANN, *Phys. Stat. Sol. (a)* **35** (1976) 347.
8. M. ALLIBERT, C. CHATILLON, J. MARESHAL

and F. LISSALDE, *J. Cryst. Growth* **23** (1974) 289.
9. J. RABIER and P. VEYSSIÈRE, unpublished work.
10. J. RABIER, H. GAREM and P. VEYSSIÈRE, *J. Appl. Phys.* **47** (1976) 4755.
11. J. RABIER, P. VEYSSIÈRE, H. GAREM, and J. GRILHÉ, *Phil. Mag. A* **39** (1979) 693.
12. G. SIMMONS and H. WANG, in "Single Crystal Elastic Constants and Calculated Aggregate Properties" (MIT Press, Massachusetts, 1971) p. 29.

Received 3 July
and accepted 17 August 1981